Measurement of Gas Temperature Profile in Discharge Region of Excimer Laser with Laser Schlieren Method

1993 Jpn. J. Appl. Phys. 32 4980

(http://iopscience.iop.org/1347-4065/32/11R/4980)

Jpn. J. Appl. Phys. Vol. 32 (1993) pp. 4980–4986
Part 1, No. 11A, November 1993

Measurement of Gas Temperature Profile in Discharge Region of Excimer Laser with Laser Schlieren Method

Shinichiroh KOSUGI[1,2] *, Kazuo MAENO[2] and Hiroki HONMA[2]
[1] *Heavy Apparatus Engineering Laboratory, Toshiba Corporation, 20-1 Kansei-cho, Tsurumi-ku, Yokohama 230*
[2] *Department of Mechanical Engineering, Faculty of Engineering, Chiba University 1-33 Yayoi-cho, Inage-ku, Chiba 263*

(Received May 21, 1993; accepted for publication September 18, 1993)

Shock waves are generated by pulse discharges in the cavity of excimer lasers. The shock waves cause arcing, nonhomogeneous excitation of laser gas and limitation of repetition rate of a high-repetition-rate excimer laser. Distribution of temperature rise by pulse discharge is an essential factor for generation and propagation of shock waves. Gas temperature profiles in the discharge region of the excimer laser cavity are measured by a laser schlieren method for single-pulse operations. The results show that the temperature distribution depends on the xenon concentration. In the cases of pure helium and higher xenon concentration, the temperature distributions are steeper than those in the cases of lower xenon concentration.

KEYWORDS: temperature measurements, energy distribution, excimer laser, TEA-CO_2 laser, laser schlieren

1. Introduction

High-repetition-rate excimer lasers are expected to be useful for wide industrial applications, such as surface treatments and minute manufacturing. The powers of present excimer lasers, however, decrease in higher repetition-rate operations.[1,2] Nowadays, the repetition rate of existing excimer lasers is limited up to 4 kHz.[2] Shock or acoustic waves, which are caused by the periodic pulse discharges, are considered to limit the repetition rate of the excimer laser. Such waves cause inhomogeneity of gas density in the discharge region of the excimer laser, which affects the successive pulse discharge, resulting in harmful disturbances. In order to avoid the effect of the shock waves, a shock-wave-damper system has been adopted in a high-repetition-rate excimer laser.[1] The repetition rate of the laser is improved with the application of the damper system. The detailed behavior of the waves, however, has not been clarified yet, so it sometimes causes mismatching between the rates and the laser powers.

A conventional Chang electrode system[3] is usually applied to high-repetition-rate excimer lasers. The Chang electrode system does not produce uniform glow discharge. The system causes concentration of discharge at the center of the discharge band. The repetition rate was improved by the adoption of an advanced electrode system that provided more uniform glow discharge.[4] In the case of the transversely excited atmospheric (TEA)-CO_2 laser, the repetition rate was improved from 175 Hz to 350 Hz with use of the advanced electrode system.[4] The temperature rise caused by the concentration of discharge energy can be lowered with the application of the more uniform glow discharge. Furthermore, the efficiency could also be improved by the application of the uniform discharge.

In general, the intensity of shock waves depends on the temperature rise of the gas heated by the discharge energy release, that is, lower temperature increase yields lower Mach number of the wave.[5,6] Generation and propagation of the shock waves in the cavity of the excimer laser are connected to the energy distribution of the discharge. Therefore, in order to study the problem of the shock waves in the laser cavity, it is very important to establish the temperature distribution in the discharge region. However, direct measurement of the temperature distribution of the discharge region is very difficult. In order to study the density fluctuation in the cavity of excimer lasers, interferometric methods were applied by Delaporte *et al.*[1] However, the treatment of the interferometric results is rather difficult and inaccurate, because the space resolution is not sufficient to obtain a precise distribution. In this paper we present a laser schlieren method to measure the temperature distribution. Using this method, we can obtain spatially integrated two-dimensional temperature distribution. The accuracy of this method is discussed, and typical results for our experimental model of the excimer laser cavity are also discussed.

2. Laser Schlieren Method

Figure 1 shows the schematic diagram of the laser schlieren method.[7,8] A He-Ne laser beam passes through the test section. The refraction angle of the He-Ne laser

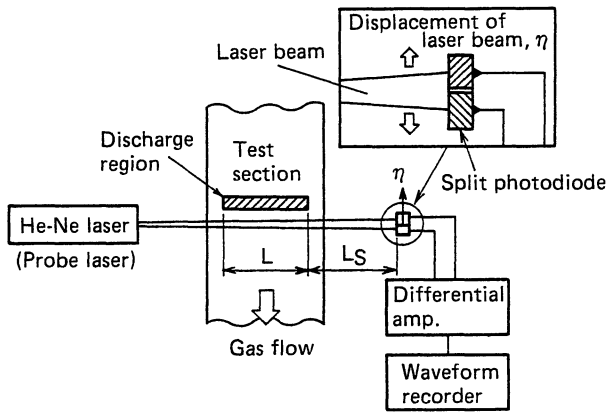

Fig. 1. Schematic diagram of laser schlieren method.

*e-mail adress: kosugi@fnkiki1.keihin.toshiba.co.jp

beam is proportional to the gas density gradient which is perpendicular to the beam. In our experiment the refraction angle of the He-Ne laser is measured using a split photodiode. In the case of the Gaussian beam, the power distribution of the laser beam is expressed as

$$P(x,y) = P_0 \left(\frac{2}{\pi a^2}\right) \exp\left(-\frac{2(x^2+y^2)}{a^2}\right), \quad (1)$$

where P_0 is the total energy of the laser beam, and x and y are the axes wherein the origin is set at the center of the beam. The radius a of the laser beam is a function of distance D measured from the laser outlet, as

$$a = a_0 \left(1 + \left(\frac{\lambda D}{\pi a_0^2}\right)^2\right)^{0.5}, \quad (2)$$

where λ is the wavelength of the laser and a_0 is the laser beam waist (e^{-2} radius). The refractive index of gases increases with increasing gas density. Laser light curves toward the higher-density direction according to the change of the density gradient. The laser spot on the split photodiode is moved to the corresponding side. Let the position of the laser spot center measured from the center of the split photodiode be η. The power incidents to the respective diode on the split photodiode are expressed by

$$I_1 = \int_{-W/2}^{W/2} \int_{-\eta}^{W} P(x,y)dxdy, \quad (3)$$

$$I_2 = \int_{-W/2}^{W/2} \int_{-W}^{-\eta} P(x,y)dxdy, \quad (4)$$

where W is the size of each sensor of the split photodiode. The difference can be expressed as

$$\Delta I = I_1 - I_2 = f(\eta). \quad (5)$$

The difference ΔI can be measured as the output voltage of the split photodiode. The relation of $f(\eta)$ is determined experimentally, as mentioned in §3. By using the relation of $f(\eta)$, η can be determined. The spatial resolution of this method depends on the laser beam radius. The changes of refractive index which occur within the spot of the laser beam cannot be resolved accurately. These changes of the refractive index affect the shape of the laser spot on the split photodiode. Narrowing the laser beam affords a high spatial resolution. Typical beam radius a_0 of the He-Ne laser ($\lambda = 0.6328$ μm) is 0.2 mm to 0.65 mm. In the case of $a_0 = 0.5$ mm, the beam radius a becomes 0.64 mm 1 m from the laser exit. The reduction of the laser beam radius yields a larger extension angle of the beam. In the case of $a_0 = 0.2$ mm, the beam radius a becomes 1.02 mm at the same distance. In order to improve spatial resolution, we must focus the laser beam. In our experiment, the He-Ne laser with a 0.42 mm beam waist is used without a lens system. The beam radius of the laser is kept under 0.5 mm in our test section, and this provides sufficient spatial resolution for our purpose.

Figure 2 shows a photograph of the split photodiode (Mori-rika silicon pin photodiode MI-33H-2D). Each sensor of the split photodiode has the dimensions of 3 mm × 3 mm (W = 3 mm). Figure 3 shows the plot of the output of the split photodiode sensor against the center position of the laser spot on the sensor. In order to obtain the output of the split photodiode as DC voltage, an amplifier system which transforms the output current of the photodiode into DC voltage is developed. The sensor is placed on the bench with a micrometer in order to move the sensor as needed. The split photodiode is moved using the micrometer. In order to obtain the relation of $f(\eta)$, the DC voltage output of the split photodiode and the values of the micrometer are measured. The plot in the figure shows the results, and the solid line shows $f(\eta)$ which is a fifth-order polynomial fitted using the least squares method. Using this relation, we determine the displacement of the laser beam from the output voltages of the split photodiode.

The index of refraction of gas, n, is

$$n = 1 + K\rho, \quad (6)$$

where K is the Gladstone-Dale constant and ρ is gas density. If a density gradient is present, laser light curves to

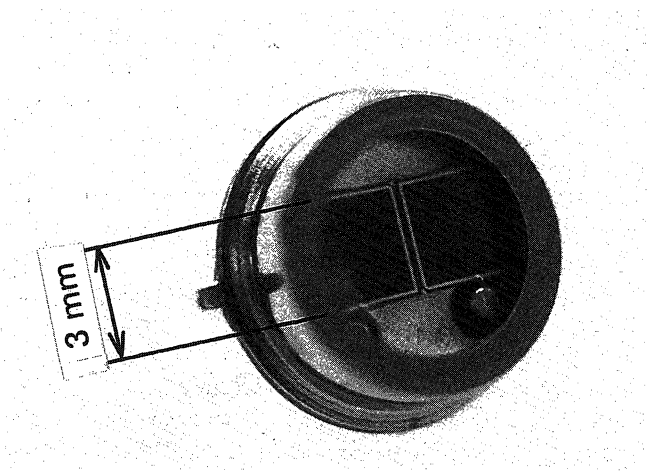

Fig. 2. Photograph of the split photodiode.

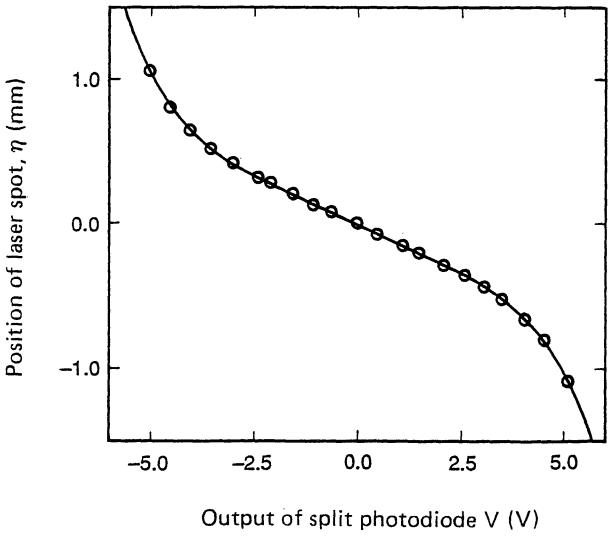

Fig. 3. Relationship between the output of the split photodiode sensor and the position of the laser beam center on the sensor.

the higher-density direction. Let the refractive angle of laser light be Θ. Passing the laser light through the test section makes Θ be

$$\Theta = K\frac{L}{n}\overline{\frac{d\rho}{dx}}, \tag{7}$$

where $\overline{d\rho/dx}$ is the density gradient as an integral average with respect to the distance along the light path in the test section.

Θ is calculated from the displacement η of the laser spot using a geometric relation,

$$\Theta = \frac{\eta}{\frac{L}{2} + L_s}, \tag{8}$$

where L_s is the distance between the sensor and the test section (see Fig. 1). If the density gradient is not constant along the laser beam in the test section, the spatially averaged density gradient is measured in this arrangement.

3. Experimental

Figure 4 indicates the schematic diagram of the excimer laser cavity. The main electrodes consist of the upper anode and the lower cathode of 300 mm length. The Chang type is employed for both electrodes.[3] The electrodes are designed such that the discharge width is 10 mm. The pin electrodes for preionization are on both sides of the main electrodes. This discharge section model is placed in the laser chamber with windows in order to pass the probe laser beam.

Figure 5 shows a schematic diagram of the laser chamber. This chamber provides a small fan system to circulate gas. The gas in the chamber flows at a low velocity of about 8 m/s through the gap between main electrodes. The hot gas heated by the discharge is carried away from the discharge region by the gas flow. The probe laser beam (He-Ne laser) for the laser schlieren method is located 10 mm downstream of the discharge region. The discharge of the excimer laser lasts only 100 ns, typically. The gas in the discharge region is heated instantaneously. Then the heated gas expands for about 10 μs after the discharge, and the temperature and density distributions are formed. The moving hot gas with density distribution crosses the laser beam. The refractive index of gas is related to gas density by eq. (6). The laser beam bends in the direction of the higher side of refractive index. Then the refraction angle of the laser light is detected by our laser schlieren method. The density gradient is calculated from the displacement of the laser beam by using eqs. (7) and (8). The temporal gas density at the laser beam position is calculated by integrating the density gradient as

$$\rho = \rho_b + \int_0^t \left(\overline{\frac{d\rho}{dx}}\right) v dt, \tag{9}$$

where t is the time after the pulse discharge, and ρ_b and v are initial density and gas flow velocity, respectively. Gas velocity v is assumed to be constant. Equation (9) is rewritten as

$$\rho = \rho_b + \int_0^X \left(\overline{\frac{d\rho}{dx}}\right) dX, \tag{10}$$

where $X(= vt)$ is the distance between the probe laser and the upwind position at the moment of discharge. In our laser schlieren method, the gas velocity can also be measured. The period Δt during which the center of the hot gas reaches the probe laser position is detected. The velocity of the gas is calculated as

$$v = d/\Delta t, \tag{11}$$

where d is the distance between the center of the discharge region and the probe laser.

The test gas in the discharge region expands corresponding to the temperature rise due to the discharge energy. The density distribution which is calculated using eq. (10) is based on the length X after the expansion of the gas. The original length of the heated gas, X_c, is given by using the mass conservation law, as

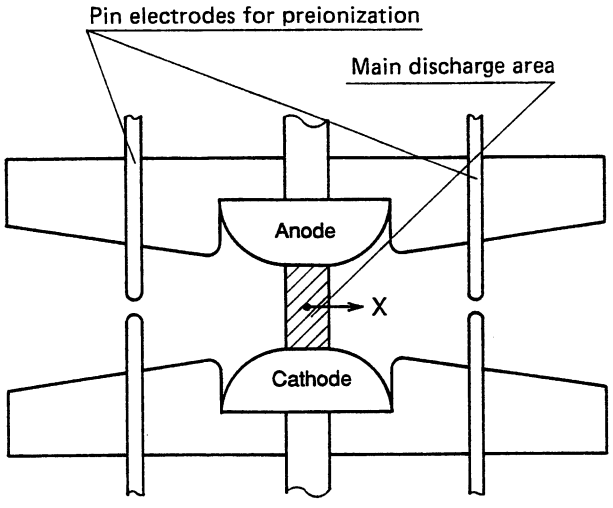

Fig. 4. Schematic diagram of the excimer laser cavity.

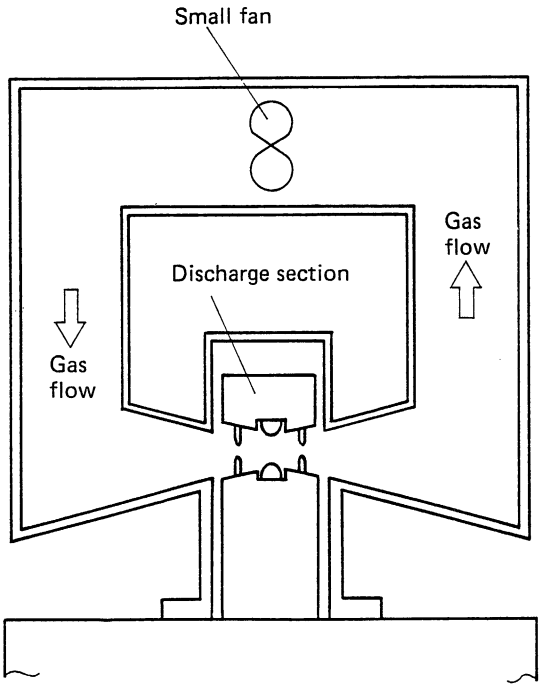

Fig. 5. Schematic diagram of the excimer laser chamber.

$$X_c = \frac{1}{\rho_b}\int_0^X \rho d\chi. \tag{12}$$

We assume that the expansion of the gas is isentropic. The original temperature of the heated gas is calculated as

$$T_c = \left(\frac{\rho_b}{\rho}\right)^{\gamma-1} T_b, \tag{13}$$

where γ is the ratio of specific heats and T_b is the initial temperature.

The probe laser beam can be positioned at any point from the center of the discharge region to 40 mm downstream, in our experimental apparatus. Consider that the probe laser beam is 10 mm downstream of the center of the discharge region in the case of that the discharge region is 10 mm wide and the gas velocity is 10 m/s. Then 1.5 ms is needed for the passage of the high-temperature gas.

$$t = (10 + 10/2)/10/1000 = 1.5 \text{ ms} \tag{14}$$

During the 1.5 ms period, such a possibility may occur that the shape of the temperature distribution is deformed by the effect of heat conduction. This problem will be discussed in the next section. Furthermore, in that period of time, the electron density decreases to a level where it does not affect the Gladstone-Dale constant.[9,10] The electron density is estimated to be $10^9/\text{cm}^3$ (10^{-5}%) 1 ms after the discharge. Hence the Gladstone-Dale constant can be calculated as[11-13]

$$K_m = \frac{\sum m_i P_i K_i}{\sum m_i P_i} \tag{15}$$

where m_i, K_i, and P_i are the molecular weight, the Gladstone-Dale constant and the pressure of i-species, respectively.

Figure 6 shows the electric circuit in which the gap switch (G.P.), 20.7 nF main capacitor (Cs), 11.9 nF peaking capacitor (Cp), and 126 μH coil (L) are employed. In the case of 20 kV DC supply voltage, the energy E stored in the main capacitor Cs is

$$E = \frac{1}{2}C_S V^2 = 4.14 \text{ J}, \tag{16}$$

where V is the DC supply voltage for the main capacitor.

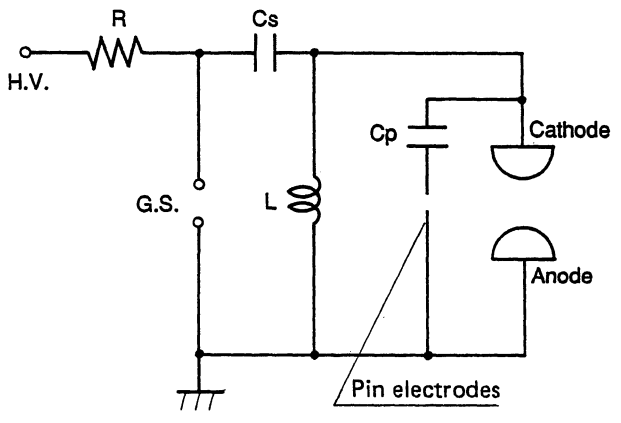

Fig. 6. Electric circuit diagram.

The energy deposition is about 70 J/L (=330 J/Kg for 1000 Torr pure helium) in the discharge region.

4. Results and Disscusion

Figures 7(a), 7(b) and 7(c) illustrate the histories of the laser beam displacement η after the discharge measured at 5 mm, 10 mm and 15 mm downstream of the discharge center, respectively. These histories of the laser beam dis-

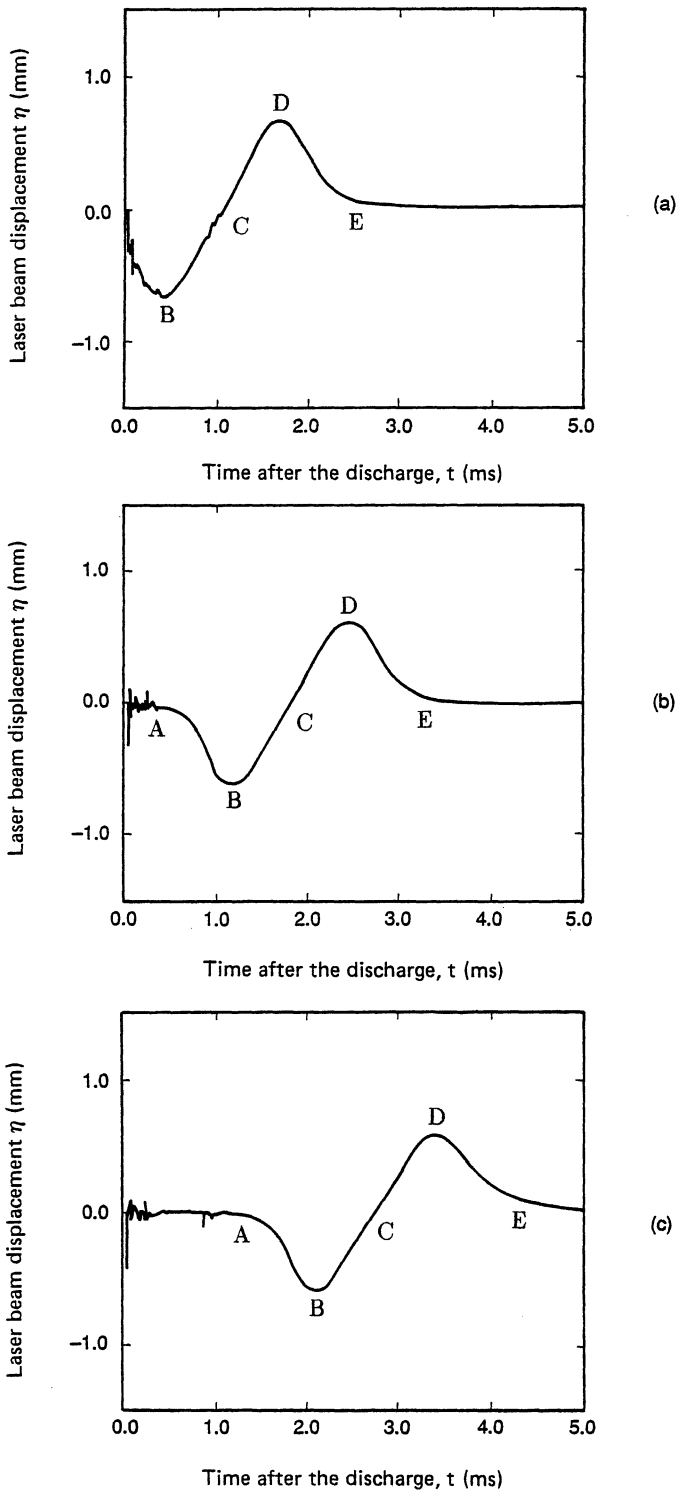

Fig. 7. History of the probe laser displacement.
(a) Probe laser beam positioned 5 mm from discharge center.
(b) Probe laser beam positioned 10 mm from discharge center.
(c) Probe laser beam positioned 15 mm from discharge center.

placement are for the case of 1000 Torr pure helium and 4.14 J discharge energy (20 kV discharge voltage). The laser beam displacement is related to the density gradient as discussed in §3. The histories are transformed to the density gradient history. In these figures, negative values of the laser beam displacement represent negative values of the density gradient. Thus the negative values of the laser beam displacement represent decreasing gas density at the laser beam position. The curves initially decrease and reach the minimum values (point B). Then they increase and exceed the zero value at point C which corresponds to the center of the hot gas, and reach the maximum values (point D). At point C, the density becomes a minimum value. The gas velocity can be calculated using eq. (11), with the time at point C and the distance between the discharge center and the probe laser.

From comparison of the three histories of laser beam displacement, it is clearly seen that the preceding negative parts (A–C) show the same patterns in all three cases. The subsequent parts that indicate positive values are slightly different. In these three traces of Fig. 7, the minimum values (point B) are the same, but the maximum values (point D) decrease with increasing distance between the discharge center and the probe laser beam. This decrease of the maximum values is caused by the effect of heat conduction of the hot gas. It can be concluded that the heat-conduction effect of the first half (A–C) of the displacement η is small enough to calculate the temperature distribution under the assumption of isentropic change of the heated gas. If the discharge energy distribution (temperature distribution) is assumed to be symmetrical with respect to the center of the discharge region, we can determine the overall temperature distributions by using the initial negative part of the displacement η. The data for 10 mm downstream of the discharge center are adopted in order to determine the temperature distribution. The small notches on the curves are caused by shock waves, thus if the time scale is enlarged we can also obtain the density gradient in the pressure waves. In order to calculate the temperature distributions, the displacement curve is smoothed by using a numerical filter function.

Figure 8 shows the temperature distribution which is mentioned above in the case of 1000 Torr pure helium. The solid line in Fig. 8 indicates the temperature distribution calculated using the negative part of the laser beam displacement η which is shown in Fig. 7(b). The horizontal axis indicates the distance measured from the center of the discharge region. From this figure the temperature rise at the center of the discharge reaches 143 K. The temperature rise extends from $X_c = -5$ mm to $X_c = 5$ mm. In order to estimate the effect of heat conduction, the heat-conduction equation is calculated. The temperature changes in directions other than the X direction are negligibly small. In the calculation it is assumed that the heat conduction occurs one-dimensionally in the X direction. The broken line in Fig. 8 shows the temperature distribution after 1 ms of the discharge which is calculated assuming the initial distribution to be the solid line in Fig. 8. The calculated result shows that the effect

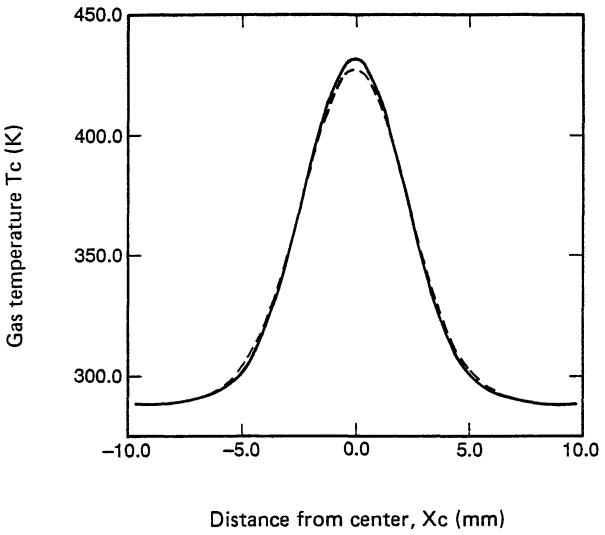

Fig. 8. Temperature distribution in the case of 1000 Torr pure helium. (Solid line: the measured result; Broken line: the numerical result after 1 ms of discharge which is calculated with heat-conduction equation assuming the initial distribution to be the solid line.

of the heat conduction is small. The effect of thermal radiation is considered to be less than the effect of heat conduction. The emissivity of one-atom gas is negligible in low temperature.

The energy needed to heat the gas in the discharge region can be calculated as

$$E = \int C_v \rho_b \Delta T A dX, \tag{17}$$

where C_v is specific heat at constant volume, ΔT is gas temperature rise and A is discharge region (gap×length). In the case of Fig. 8, 3.38 J is consumed to heat the gas, and 90% of the energy is concentrated in the range of $|X_c| < 3.6$ mm.

Figure 9 shows the temperature distribution for the case of the mixture of 1 Torr xenon and 1000 Torr helium. By adding 1 Torr xenon, temperature rise became 96 K, which is about 2/3 of the pure helium case. Also, the heating region caused by the discharge is wider than in the pure helium case. Ninety percent of the energy is consumed within the range of $|X_c| < 4.7$ mm. Figures 10 and 11 are the results for 5 Torr xenon and 30 Torr xenon cases. With the increase of xenon concentration, the temperature distribution becomes steeper again. In the case of the mixture of 5 Torr xenon and 1000 Torr helium, the maximum temperature rise is 98 K, and 90% of the energy is consumed within the range of $|X_c| < 4.2$ mm. In the case of the mixture of 30 Torr xenon and 1000 Torr helium, the maximum temperature rise reaches 143 K, and 90% of the energy is concentrated to the range of $|X_c| < 2.8$ mm.

Figure 12 shows the plot of the energies against the xenon pressure. The energies are calculated by using eq. (17). In the case of pure helium, more energy is consumed for main discharge. In the cases of the mixture of xenon and helium, the energy consumption shows a constant value. It is considered that the difference in the consumed energy is caused by the difference in the dis-

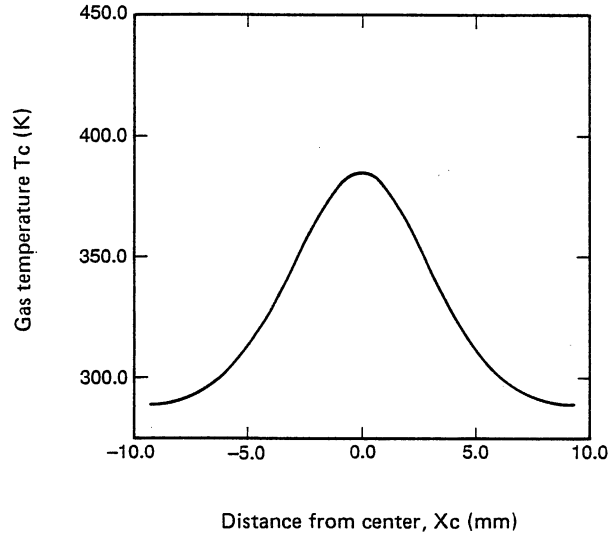

Fig. 9. Temperature distribution in the case of 1 Torr xenon and 1000 Torr helium.

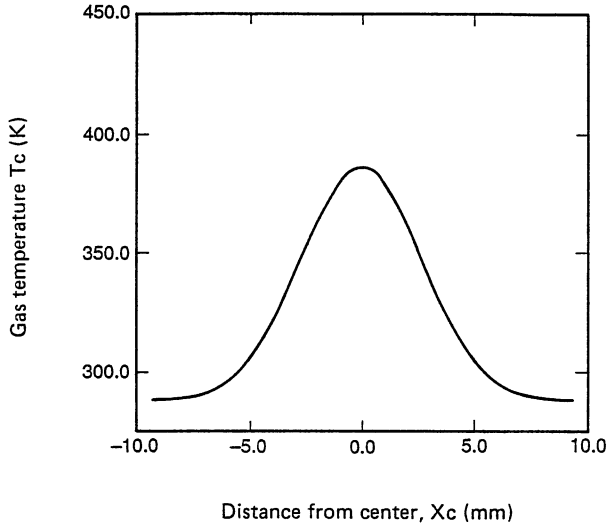

Fig. 10. Temperature distribution in the case of 5 Torr xenon and 1000 Torr helium.

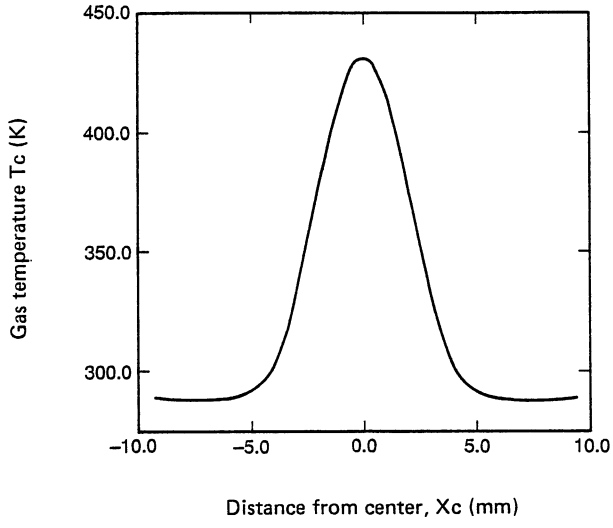

Fig. 11. Temperature distribution in the case of 25 Torr xenon and 1000 Torr helium.

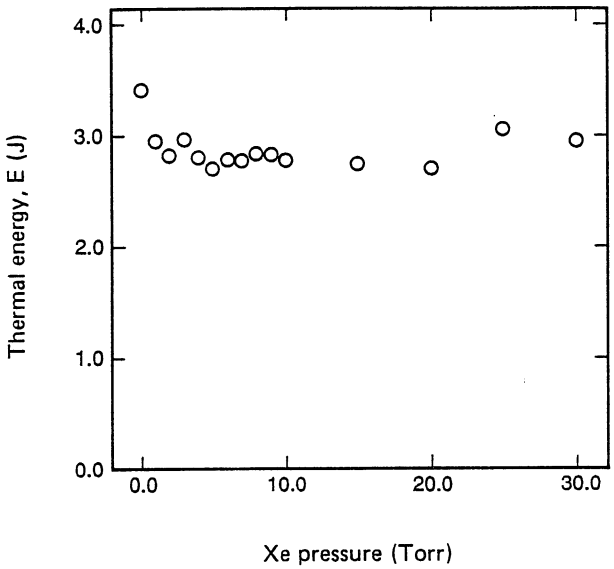

Fig. 12. Plot of energy against the Xe pressure.

charge characteristics. In the case of the mixed gas, the voltage required to maintain the discharge is larger than the value of pure helium.

From these results, we can conclude that the Chang electrode system is not always suitable for excimer laser application. The energy in the outskirts of the discharge region is not utilized for laser output, and the discharge energy is concentrated in the center portion of the discharge region, so that the gas in the center region is heated strongly. For the high-repetition-rate excimer laser, it is advantageous to adopt an electrode system which provides the uniform and narrow energy distribution.

Density variation must be eliminated from the discharge region to start the subsequent discharges. The outskirts of the discharge region, which are not effective for laser output, must also be removed. A uniform and narrow distribution of discharge energy helps to eliminate density variation. Furthermore, the most appropriate shape of the electrodes can be designed for specific xenon concentrations, using our experimental results.

5. Conclusions

Temperature distribution in the discharge region of the excimer laser cavity is measured by use of a laser schlieren method for the case of single pulse operation. The method to measure temperature distribution utilizes diffraction of the laser beam within the motion of discharged hot gas. If the probe laser beam is positioned just next to the discharge region and first half of laser beam diffraction changes are used, the effect of the diffusion is small enough to allow calculation of the temperature distribution. This technique can be used for temperature measurement in the case of high-repetition operation. The temperature distributions can be utilized for numerical studies of the generation and propagation of the shock waves in the cavity of the excimer laser.

The results show that the temperature distribution changes with the increase of xenon concentration. In the

case of pure helium, 90% of the thermal energy exists within the range of $|X_c| < 3.6$ mm. By adding 1 Torr xenon to the pure helium gas, the thermal range where 90% of the thermal energy exists becomes $|X_c| < 4.7$ mm. In the case of the mixture of 30 Torr xenon and 1000 Torr helium, the thermal range decreases to $|X_c| < 2.8$ mm. In the cases of low xenon concentration, the region where the hot gas exists is broad. In such cases, a relatively long period between the discharge pulses is needed to remove the hot gas from the discharge region by gas flow.

Acknowledgements

The authors would like to express their thanks to Professor Schgaev of Moscow State University, Mr. Koreeda of Chiba university and Dr. Takagi of Toshiba Corporation for their helpful advice. Part of this work was conducted within the program 'Advanced Material-Processing and Machining System,' consigned to the Advanced Material-Processing and Machining Technology Research Association from the New Energy and Industrial Technology Development Organization, which is carried out under the Large-Scale Project enforced by the Agency of Industrial Science and Technology, the Ministry of International Trade and Industry.

1) P. Delaporte, B. Fontaine, B. Forestier, M. Sentis, J.-P. Truong, O. Uteza, D. Zeitoun and D. Tarabelli: Proc. 18th Int. Symp. Shock Waves, 1991 (1992) Vol. 2, p. 1301.
2) T. Goto, S. Takagi, N. Okamoto, K. Kakizaki and S. Sato: Proc. SPIE **1810** (1993) 376.
3) T. Y. Chang: Rev. Sci. Instrum. **144** (1973) 405.
4) A. Ishii, Y. Okita, K. Yasuoka, T. Tamagawa, S. Nakagawa, I. Ohshima: Jpn. J. Appl. Phys. **32** (1993) 75.
5) S. Kosugi, K. Maeno and H. Honma: Proc. SPIE **1810** (1993) 217.
6) S. Kosugi, T. Ohishi, K. Maeno and H. Honma: Proc. 18th Int. Symp. Shock Waves, 1991 (1992) Vol. 2, p. 1295.
7) J. H. Kiefer and J. C. Hajduk: Proc. 12th Int. Symp. Shock Waves, 1980 (1980) p. 97.
8) J. Koreeda, H. Yanagisawa, K. Maeno, H. Honma, S. A. Bystrov, V. I. Ivanov, F. V. Shugaev: to be published in Proc. 19th Int. Symp. Shock Waves, 1993.
9) M. Hiramatsu, H. Furuhashi and T. Goto: J. Appl. Phys. **60** (1986) 1946.
10) A. De Angelis, P. Di Lazzaro, F. Garosi, G. Giordano and T. Letardi: Appl. Phys. B **47** (1988) 1.
11) M. Born and E. Wolf: *Principles of Optics* (Pergamon Press, Oxford, 1964) p. 87.
12) C. W. Allen: *Astrophysical Quantities* (University of London, Athlone Press, London, 1973) p. 90.
13) *Tables of Physical and Chemical Constants* (Longmann, London, 1980) p. 99.